# Updates to the AMSR-E Level-2A Version B07 Algorithm

**Frank J. Wentz**

**January 30, 2006**

## 1. Introduction

A major update to the Level-2A algorithm was completed January 26, 2006. This update is called PGE Version B07. This document describes the changes that were made relative to the previous version B06. Note the B06 was a brief interim version that was used to process data from August 2005 to February 2006. Some of the changes discussed herein were implemented in B06 (as discussed below); however B07 represents the full implementation of all the changes discussed herein.

B07 is an important milestone in Remote Sensing Systems (RSS) algorithm development for Level-2A. The plan is to have the AMSR-E Science Team validate B07. If any modifications or additions are deemed necessary (which we expect to be minor), they will be made and the resulting final version will be called V08. At that point, the entire AMSR-E data set will be reprocessed using V08.

## 2. Changes to Geolocation Routines

We and others have recognized for some time that the AMSR-E brightness temperature imagery was misregistered relative to coastlines and other land features. The error in geolocation was about 5-7 km. The misregistration is most apparent when one differences ascending imagery from descending imagery. The ascending imagery is shifted one way and the descending imagery is shifted the other way, thereby making the problem more apparent. Figure 1 shows an example of the problem.

After some analysis, it was recognized that the misregistration was due to a misalignment of the AMSR-E sensor relative to the spacecraft. This problem was fixed by a trial-and-error method in which various roll, pitch, and yaw corrections were applied to the AMSR-E alignment until proper registration was obtained. This was done by two completely independent analyses. The first analysis done by Peter Ashcroft of RSS used the island of Kauai as a reference. The AMSR-E alignment was varied until the imagery of Kauai was co-registered with a high-resolution map of the Kauai coastline. The second analysis done by Frank Wentz relied on the ascending-minus-descending imagery like that shown in Figure 1. Left-swath minus right-swath imagery was also used. Proper alignment is obtained when the halo-like effects near coastline, rivers, and other high-contrast land and ice features go away as shown in Figure 1. Both analyses resulted in nearly the same set of adjustment parameters. A comparison of the two different approaches suggests that the accuracy of the geolocation analysis is between 1 and 2 km, which is the accuracy we now place on the AMSR-E cell locations.

A separate geolocation analysis was done for each channel (14 in all). The results show for a given frequency the v-pol and h-pol channels are well aligned. Furthermore, the 19, 23, and 37 GHz channels are also well aligned with each other. Table 1 gives the azimuth, cone, and roll angles that are required at each frequency to achieve proper geolocation.

Note that the corrections to the geolocation for channels 19 GHz through 89 GHz were implemented in Version B06. However, B06 did not include the alignment of the 7 and 11 GHz channel locations via optimum interpolations, which is discussed in the next section.

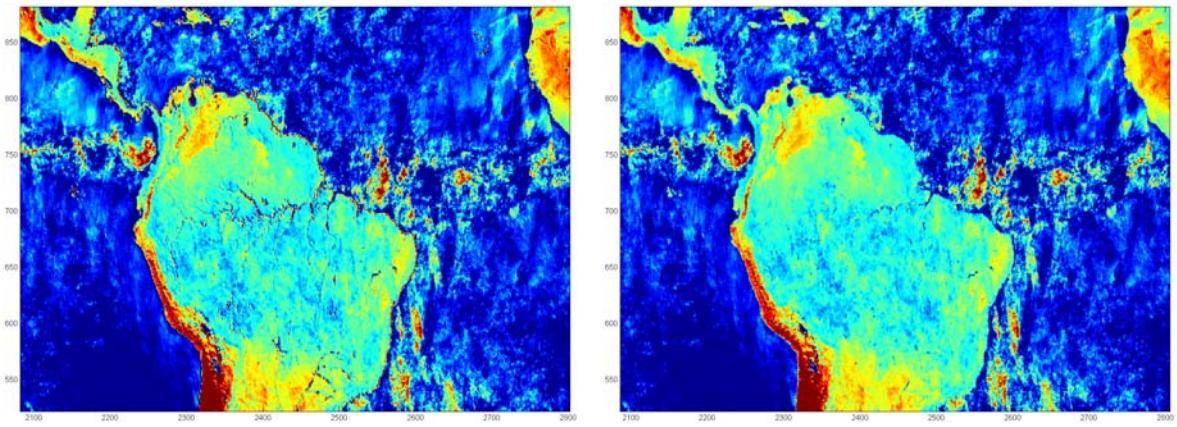

**Figure 1. An ascending minus descending difference map of AMSR-E 37-GHz imagery. In the left image you can see a halo effect near coastlines, rivers and other land features having a sharp contrast. After applying corrections to compensate for the AMSR-E misalignment, one obtains the right image.**

**Table 1. The Alignment Angles for AMSR-E Deduced from the Geolocation Analysis**

| Channel | Azimuth angle (deg.) | Cone angle (deg.) | Roll angle (deg.) |
|---|---|---|---|
| **7 GHz** | -74.838 | 47.67 | 0.09 |
| **11 GHz** | -74.948 | 47.64 | 0.09 |
| **19 GHz** | -74.948 | 47.57 | 0.09 |
| **24 GHz** | -74.948 | 47.57 | 0.09 |
| **37 GHz** | -74.948 | 47.57 | 0.09 |
| **89 GHz A** | -75.148 | 47.57 | 0.09 |
| **89 GHz B** | -75.424 | 47.09 | 0.09 |

## 3. Resampling 7 and 11 GHz channels to Match Locations for Higher Frequencies

The analysis discussed in the previous section showed that the 7-GHz and the 11-GHz horns are pointing in a slightly different direction than the 19-23-37 GHz horns. Rather than providing a separate set of latitudes and longitudes for 7 GHz and another set of 11 GHz, we decided it would be more useful to resample the 7 and 11 GHz observations in such a way as to match the location of the higher frequencies. Since these channels are being resampled anyway, it makes sense to adjust the resampling weights so that the resampled $T_A$ at 7 and 11 GHz match the location of the higher frequencies. This required rederiving the sampling weights, this time with the center of the target cell positioned at the location of the 19 GHz channel rather than at the 7 or 11 GHz footprint position. One drawback is that the un-resampled 7 and 11 GHz observations are missing an exact specification of latitudes and longitudes. Figure 2 gives an example of the improvement in the Version B07 7-GHz imagery.

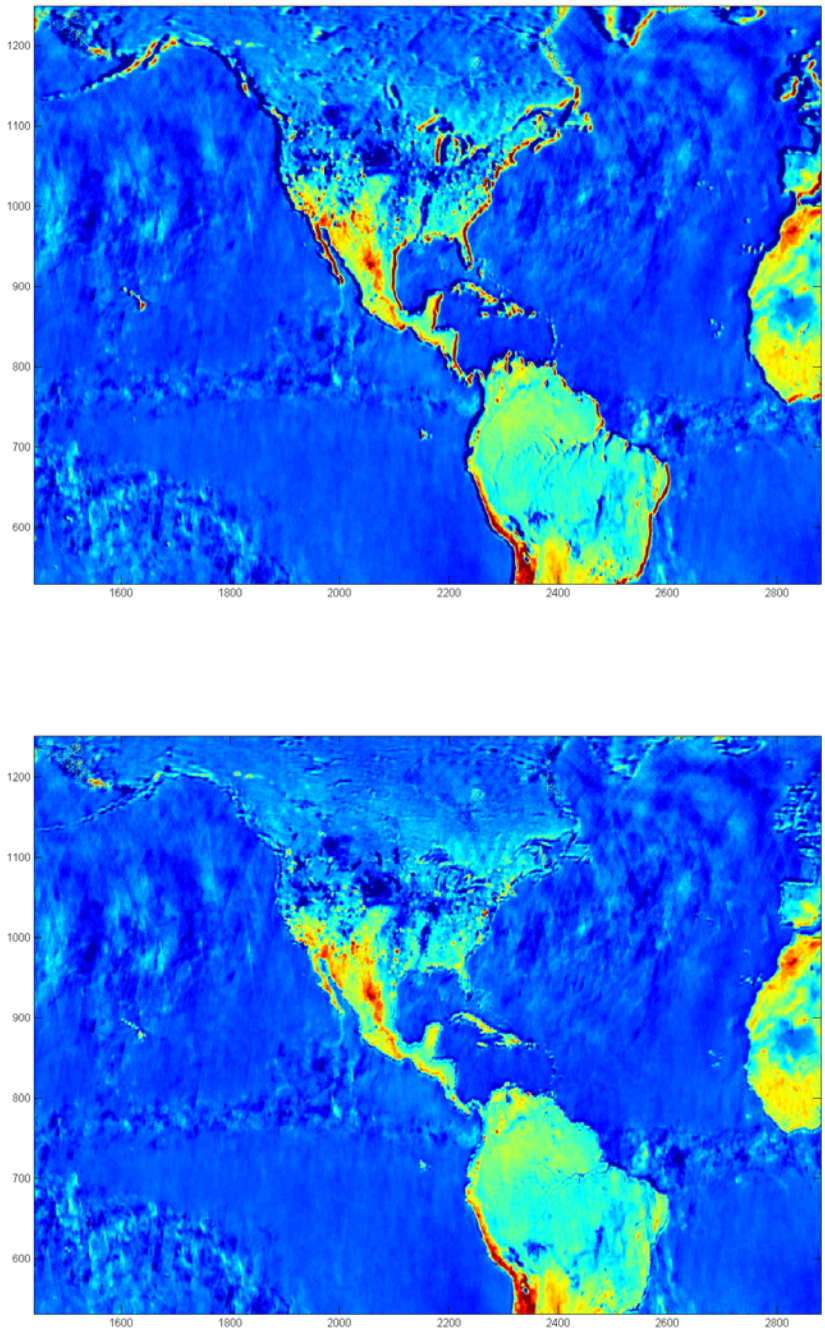


**Figure 2. An ascending minus descending difference map of AMSR-E 7-GHz imagery. The top image is with the old geolocation parameters and the old resampling weights that did not adjust the location of the imagery. The bottom image is with the new geolocation parameters and the new resampling weights that align the 7-GHz imagery with the 19-GHz imagery. One can see the halo effect near coastlines, rivers and other land features is much less in the bottom image.**

## 4. Revised Method for Computing the Effective Temperature of the AMSR-E Hot Load

An on-orbit calibration is required for AMSR-E because of a design flaw in the AMSR-E hot load. For our initial method, the effective temperature of the AMSR-E hot load was estimated using the existing network of satellite radiometers. Remote Sensing Systems maintains a real-time database of daily observations from U.S. operational and research satellites. These satellite retrievals of sea-surface temperature (SST), wind, vapor, and cloud water were collocated in time and space with the AMSR-E observations. The collocated observations were then processed by a radiative transfer model (RTM) that computes the intensity of radiation entering the AMSR-E feedhorns. In essence, this process provides an earth-target calibration point. A 2-point linear extrapolation based on the cold mirror and earth-target calibration points yields the desired quantity: the effective temperature of the hot load $T_{eff}$.

Although this old method of computing $T_{eff}$ worked well, there were drawbacks. The method requires collocated SSM/I and TMI observations. From an operational standpoint, this requirement adds considerable complexity to the Level 1 processing. The processing needs to wait for the ingestion and processing of SSM/I and TMI data. Gaps or delays in the SSM/I and/or TMI data stream are difficult to handle, and the waiting can sometimes cause a long delay in processing the ASMR-E data. From an algorithm standpoint, the spatial distribution of the SSM/I and TMI collocations is not global and can vary month-to-month. This variability in the collocation geometry may be introducing small errors into the calibration procedure. Clearly, it would be desirable to have a hot load calibration procedure that does not rely on other satellites.

The primary reason SSM/I and TMI are required is to specify the water vapor and cloud water. The other two relevant parameters, SST and wind, can be obtained with sufficient accuracy from NCEP Final Analysis fields. In order to remove the dependence on the SSM/I and TMI vapor and cloud retrievals, we modified the way in which $T_{eff}$ is computed. This new method is based on the assumption that $T_{eff}$ does not depend on polarization (i.e., it is the same for v-pol and h–pol). This assumption seems to be valid based on both empirical data (v-pol and h-pol $T_{eff}$ coming from the SSM/I-TMI method are similar) and physical considerations (hot-load is an unpolarized source). Under this assumption, the method can be modified to make it insensitive to the specification of vapor and cloud, as is now described.

The first step of the process is to estimate a value of $T_{eff}$ for each AMSR-E observation. The following expression is used to estimate the effective temperature:

$$T_{eff,i} = T_C + \rho_i \left( T_{Ai,rtm} - T_C \right) \tag{1}$$

where $T_C$ is the brightness temperature for the cold space observation and $T_{Ai,rtm}$ is the antenna temperature computed from the radiative transfer model (RTM) given the ancillary information (SST, wind, vapor, and cloud). The subscript $i$ denotes AMSR channel. The term $\rho_i$ is the following ratio of the radiometer counts:

$$\rho_i = \frac{C_{Hi} - C_{Ci}}{C_{Ei} - C_{Ci}} \tag{2}$$

where subscripts $C$, $H$ and $E$ denote cold-space counts, hot-load counts, and earth-viewing counts, respectively. Equation (1) is a linear extrapolation based on the cold-calibration point and the earth-calibration point.

The next step is to form a linear combination of effective temperatures that is relatively insensitive to variations in vapor, cloud, and to some degree wind. For a given frequency, this linear combination of $T_{eff}$ is represented by

$$\hat{T}_{eff,j} = [1 - \Lambda(W)] \sum_{i=1}^{10} p_{ij} T_{eff,i} + \Lambda(W) \sum_{i=1}^{10} q_{ij} T_{eff,i} \quad (3)$$

where subscript j denotes channel frequency, $p_{ij}$ and $q_{ij}$ are static regression coefficients, and W is wind speed. The summations are over the 10 AMSR channels from 7 to 37 GHz. (A slightly modified version is used for the 89 GHz channels.) The function Λ(W) smoothly goes from 0 to 1 as the wind speed goes from 3 to 11 m/s. Thus the first term in (3) corresponds to low-to-moderate winds, and the second term corresponds to moderate-to-high winds. Two wind speed terms are used because the wind speed response of the RTM is highly non-linear. The wind speed value comes from NCEP Final Analysis fields. The regression coefficients $p_{ij}$ and $q_{ij}$ are found from computer simulations so as to minimize the error in the estimation of effective temperature due to variations in wind, vapor, and cloud. The method for finding the coefficients is similar to that used to find the regression coefficients for the geophysical retrieval algorithms. In essence, (3) is an algorithm for estimating the hot load effective temperature.

The next step is to correlate $\hat{T}_{eff,j}$ with the thermistor temperatures and orbit position. This is done by using the following expression:

$$\hat{T}_{eff,j} = a_{0j} + b_{0j} \sin\alpha + c_{0j} \sin 2\alpha + \sum_{k=1}^{8} a_{kj}(T_k - 303) + b_{kj}(T_k - 303)\sin\alpha + c_{kj}(T_k - 303)\sin 2\alpha \quad (4)$$

where subscript $k$ denotes the 8 hot-load thermistors, $T_k$ are the thermistor temperatures, and $\alpha - 90°$ is the orbit position angle relative to the ascending node crossing of the ecliptic plane. There are 27 regression coefficients to be found for each frequency: $a_{kj}$, $b_{kj}$, and $c_{kj}$. These regression coefficients are allowed to vary in time. A ±150 orbit moving time window is used to specify the coefficients. The weighting function for the time window is triangular, going to zero at 150 orbits before the current orbit and 150 orbits after the current orbit. Thus, the time scale for the variation in the $a_{kj}$, $b_{kj}$, and $c_{kj}$ coefficients is approximately 10 days.

There are three additional improvements that we implemented. The first relates to the sea-surface temperature (SST) that we use the specify $T_{Ai,rtm}$. The SST values come from Reynolds' weekly Optimum Interpolation (OI) SST product. Since this SST product is a weekly value, it does not include any diurnal component. For the AMSR-E early afternoon orbit, diurnal variations in SST can be large when there are light winds. Accordingly we now apply a diurnal adjustment to the OI SST to model the diurnal variability of SST.

The last improvement is to apply a smoothing function to the estimation of the radiometer gain, which is given by

$$G = \frac{\hat{T}_{eff,j} - T_c}{C_{Hi} - C_{Ci}} \quad (5)$$

The gain is expected to vary smoothly over the orbit. Random errors in the estimation of $\hat{T}_{eff,j}$ will show up as rapid variations in $G$. A smoothing function is applied to $G$ to remove the

variability on short time scales (minutes), thereby further reducing the error in the $\hat{T}_{eff,j}$ estimation.

Note that this new method of computing $T_{eff}$ was first implemented in Version B06, but the final recalibration discussed in the next section was not completed until B07.

## 5. Recalibration of AMSR-E Hot Load and Along-Scan Adjustments

The correction of the AMSR-E geolocation problems required that the AMSR-E sensor alignment be 'rolled' relative to the spacecraft frame by 0.09°. Changing the roll of the sensor results in a change in the incidence angle. With this roll adjustment, we find that the true incidence angle varies across the swath (we had been assuming it was nearly constant). This modification of the incidence angle has small but significant effects on the AMSR-E calibration. The calibration is based on measurements of the ocean surface, and the emission from the ocean surface varies with incidence angle. We felt that the best thing to do was to completely recalibrate AMSR-E using the all the modifications that were implemented as part of Version B07. This was done, and a new hot load effective temperature ($T_{eff}$) table was found. The along-scan antenna temperature ($T_A$) adjustment also needed to be redone using the new roll angle. It was gratifying to see that with the roll correction, the along-scan errors in $T_A$ are significantly reduced, except near the swath edge where the cold mirror interferes with the field of view. In other words, the along-scan errors we were seeing (except at the swath edge) were due to the small misalignment of the sensor. The along-scan error before and after making the roll adjustment are shown in Figure 3.

Earth incidence angle is computed and included in Level-2A files in data field Earth_Incidence. These variable earth incidence angle data should be used appropriately, especially for geophysical retrievals depending upon incidence angle. Using the previously assumed constant incidence angle will likely result in along scan bias. It is important to note that the Brightness Temperature Dataset is intended to be a faithful representation of the brightness temperatures observed by the instrument. Thus, due to the sensor-to-spacecraft roll, incidence angle is variable along scan, and brightness temperatures are correspondingly variable along scan. This along scan variability in observed brightness temperatures is not removed. It is intended that along scan variability should be accounted for by using the computed Earth_Incidence.

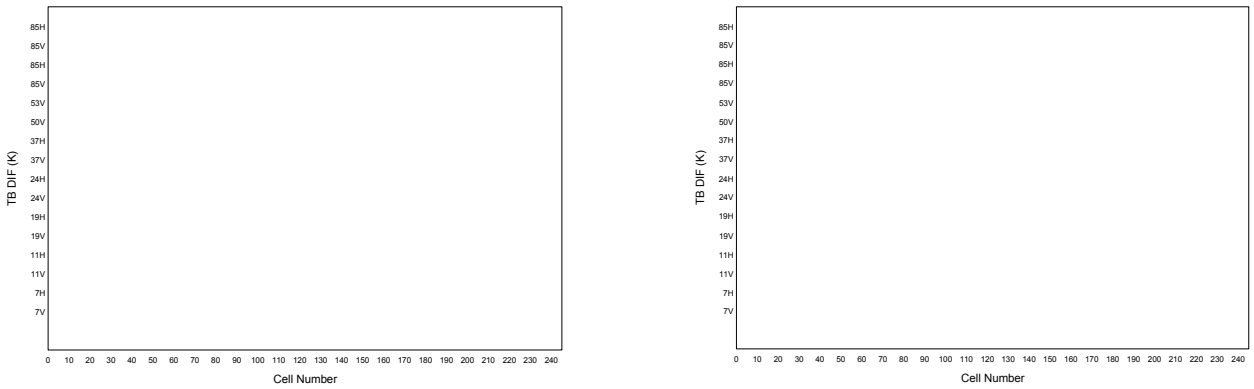


**Figure 3. The left image shows the AMSR-E along-scan errors before doing the geolocation correction. The right figure shows the error that results when the roll adjustment is made to the sensor alignment. Note that except at the swath edges (where big errors occur due to the cold mirror entering the field of view), the roll adjustment reduces the error (the curves become flatter).**

## 6. Implementation of Flagging Algorithm for RFI from Geostationary TV Satellites

As part of our SST and wind validation activity, we found anomalous retrievals off the West Coast of Europe and in the Mediterranean Sea. After some investigation, we determined that these erroneous retrievals were due to radio frequency interference (RFI) from a European satellite TV service. ASMR-E is receiving the broadcast from two European geostationary satellites that operate near the 10.7 GHz band. The satellite TV signal is reflecting off the ocean surface into the AMSR-E field of view. AMSR-E bandwidth at 10.7 GHz is 100 MHz, whereas the protected band is only 20 MHz. The TV signal is coming from the unprotected part of the 100-MHz band. Figure 4 shows the excess brightness temperature for the 10.7 GHz h-pol channel due the RFI from the TV satellites.

We determined that the TV RFI was coming from two satellites: one positioned at a longitude of 13°E above the equator and the other at 19°E. Given these longitudes and the fact that the distance from the Earth's center to a geostationary satellite is approximately 42164 km, the position of the two satellites can be determined. An algorithm was developed that computes the angle between AMSR-E look vector and the specular reflection vector for the TV RFI. This angle is called the RFI angle. Small RFI angles correspond to cases in which the TV RFI is being reflected off the ocean surface directly towards AMSR-E.

In general, we find that when the RFI angle is less than 12°, the observation should be flagged as RFI contaminated. However in the North Sea, the RFI is particularly strong. For this region, we use an RFI angle of 17° as our threshold. The North Sea area is defined as a rectangle with latitudes from 51°N to 62°N and longitudes from 3°W to 9°E. This TV RFI flagging algorithm has now been implemented into the standard AMSR-E processing. Note that the computation of the RFI angle was first implemented in Version B06.

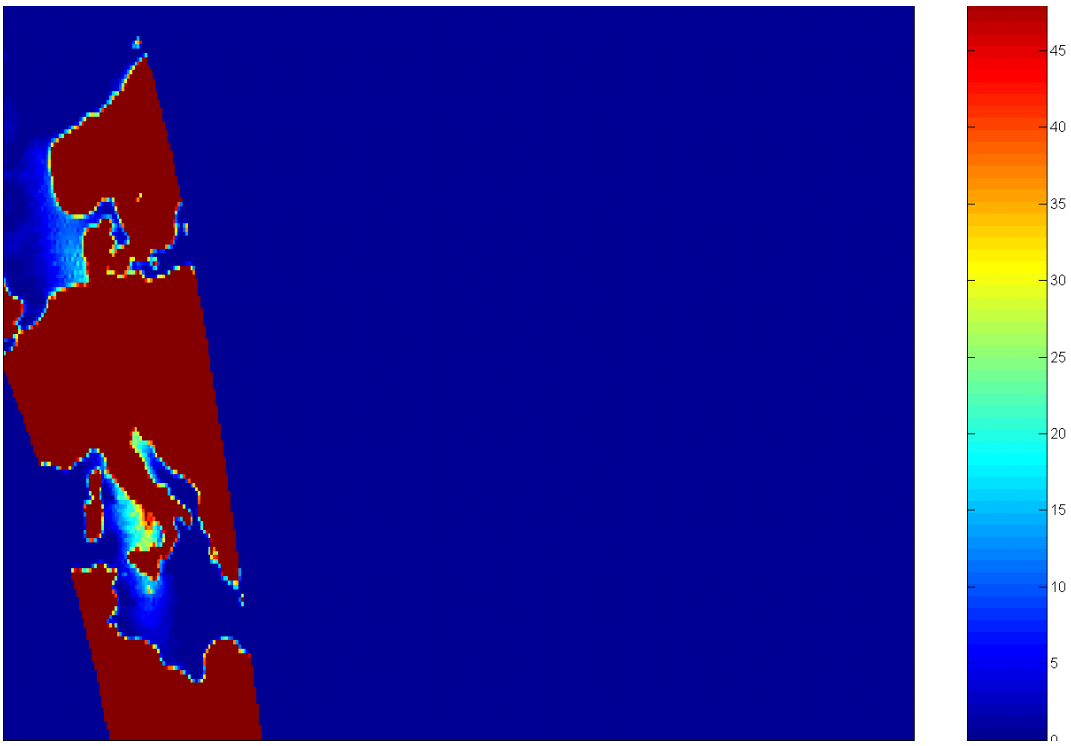


**Figure 4. Excess brightness temperature due to the reflection of TV satellite 10.7 GHz transmissions off the ocean surface.**

## 7. Correction for August-September 2003 Aqua Pitch Error

Figure 5 shows the difference between the predicted minus the definitive ephemeris satellite nadir location. The anomaly that occurs between August 12 and September 6, 2003, is due to an error in knowledge of the spacecraft pitch. This problem was due to an operator error that occurred after the August 12th Yaw Slew. In the latest JAXA L1A data, the definitive ephemeris was used for this period so the geolocation values are correct. However JAXA did not account for the fact that the anomaly caused Aqua to be inadvertently pitched during this time period. The pitch increased approximately linearly with time until the correction was made on September 6, 2003. For Version B05 and B06, we modeled the satellite pitch anomaly during this period as a ramp function: linearly increasing after August 12 and then abruptly going to zero on September 6. This is an important correction because the retrieval of SST and wind are very sensitive to incidence angle, which is directly related to pitch. On example of this is shown in Figure 6 that shows the difference in the SST retrieval before and after making the pitch correction.

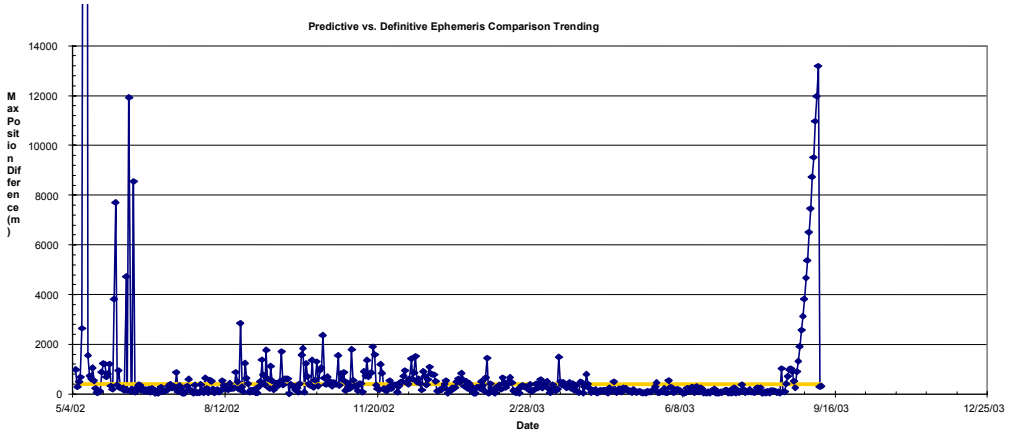


**Figure 5. Problem with Aqua pitch that occurred from August 12 to September 6, 2003**

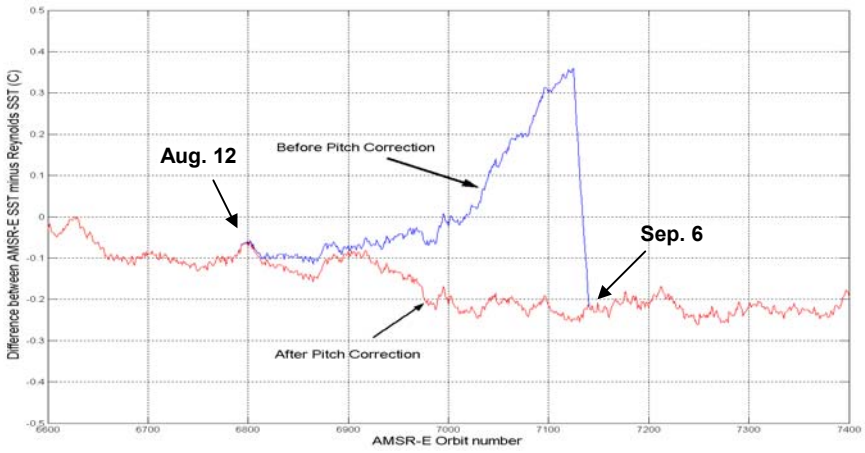


**Figure 6. AMSR-E SST retrieval minus Reynolds SST before and after applying pitch correction. The blue curve is before applying correction, and the red curve is after applying correction.**

## 8. Correction for Lunar Radiation Entering the AMSR-E Cold Mirror

Twice each month the moon enters the field of view of the AMSR-E cold mirror. The Moon's surface temperature varies from 120 K night to 370 K day and has a relatively high emissivity. As a result, the moon acts as a source of contamination to the cold sky measurement.

A correction is applied in the B07 algorithm to remove the lunar contamination. The correction depends upon the following factors:

a. The angle between the vector going from the satellite to the moon and the boresight vector of the cold mirror. This is the dominant term. When this angle becomes small (a few degrees or less), lunar contamination become significant. This angle is called the lunar angle.

b. The phase of the moon. A full moon is hotter than a new moon and hence has a higher brightness temperature.

c. The distance from the satellite to the moon. Radiation intensity falls off as the inverse of the square of the distance.

The lunar $T_A$ contribution to the cold sky observations is computed and then is scaled in terms of cold counts. The 'lunar cold counts' are subtracted from the AMSR-E cold count observations to obtain a cold count value free of lunar contamination. For the case of 89 GHz, when the lunar angle is less than 1°, the lunar contamination is too large to perform the correction, and these observations are flagged as bad and are not processed. The excluded observations are extremely rare. The accuracy of this correction is estimated to be of the order of 0.1 K.

## 9. Adjustment to Match the 89A and 89B Observations When Doing Resampling

When the 89 GHz channels are resampled to lower spatial resolutions, the observations from the A-horn and the B-horn are combined. However, the incidence angles for these two horns are different, with the B-horn incidence angle being about 0.6° smaller than the A-horn. To compensate for the difference in incidence angle, Version B07 applies the following adjustments to the A-horn measurements before resampling.

$$T_{AV,adj} = 0.130671 + 0.993251 T_{AV} \tag{6a}$$

$$T_{AH,adj} = 0.472994 + 0.992742 T_{AH} \tag{6b}$$

These expressions were found from doing linear regression of actual A-horn and B-horn observations over the first two mission years of AMSR-E. The application of these equations normalizes the A-horn measurements to the B-horn incidence angle.

## 10. Implementation of using UT1 time to compute the Earth rotation angle.

Aqua's position, velocity, and attitude vectors are given in terms of the J2000 inertial coordinate system. To compute Earth latitudes and particularly longitudes, it is necessary to compute the Earth rotation relative to the J2000 systems. The proper calculation requires using the UT1 time, which can be as much as one second different from UTC time. To obtain UT1, the L2A algorithm now accesses U.S. Naval Observatory database each day to obtain the current UT1. One advantage of this procedure is that it is independent of leap seconds. That is to say, there is no discontinuity in the geolocation parameters when a leap second occurs.